Catalysis Science & Technology

PAPER

View Article Online
View Journal | View Issue

Cite this: *Catal. Sci. Technol.*, 2014, 4, 4219

Cyclopentadienyl molybdenum alkyl ester complexes as catalyst precursors for olefin epoxidation†

Nidhi Grover, Alexander Pöthig and Fritz E. Kühn*

Received 5th June 2014,
Accepted 10th July 2014

DOI: 10.1039/c4cy00738g

www.rsc.org/catalysis

New molybdenum complexes of the type $[CpMo(CO)_3X]$ containing ligands of the formula X = $CHR^2CO(OR^1)$ where R^1 = ethyl (**1**), menthyl (**4**), and bornyl (**5**) and R^2 = H; R^1 = ethyl and R^2 = methyl (**2**) and phenyl (**3**) have been synthesized and characterized by NMR and IR spectroscopy and X-ray crystallography. These compounds have been applied as catalyst precursors for achiral and chiral epoxidation of unfunctionalized olefins with *tert*-butyl hydroperoxide (TBHP) as the oxidant at 22 °C (in CH_2Cl_2) and 55 °C (in $CHCl_3$). The substrates *cis*-cyclooctene, 1-octene, *cis*- and *trans*-stilbene, and *trans*-β-methylstyrene were selectively and quantitatively converted into their epoxides using a catalyst : substrate : oxidant ratio of 1 : 100 : 200 within 4 h at room temperature in CH_2Cl_2 and within 15 min at 55 °C in $CHCl_3$. Complexes **1**–**5** are precursors of active epoxidation catalysts and turnover frequencies (TOFs) of *ca.* 1200 h^{-1} are obtained with *cis*-cyclooctene as the substrate. No enantioselectivity is observed with *trans*-β-methylstyrene as the substrate despite the application of enantiomerically pure precatalysts. *In situ* monitoring of catalytic epoxidation of *cis*-cyclooctene with complex **5** by ^1H and ^{13}C NMR spectroscopy suggests that the chiral alkyl ester side chain is retained during oxidation with TBHP. During epoxidation, the primary catalytic species is the dioxo complex $[CpMoO_2X]$. After near complete conversion of *cis*-cyclooctene to its epoxide, further oxidation of the dioxo complex to oxo–peroxo complex $[CpMo(\eta^2\text{-}O_2)(O)X]$ takes place. The oxo–peroxo complex is also an active epoxidation catalyst.

Introduction

Since the development of the Halcon–ARCO process for industrial propylene oxide production using molecular Mo(VI) catalysts and organic hydroperoxides in the homogeneous phase, improvements in stability, selectivity and applicability of specialized molybdenum complexes for homogeneous and heterogeneous epoxidation catalysis have been focal points of studies.[1] Mononuclear complexes such as $[MoO_2X_2L_n]$ (X = halide, alkyl, siloxy; L = mono- or bidentate ligand),[2–6] $[\eta^5\text{-}(C_5R_5)Mo(CO)_3X]$ (R = H, CH_3, CH_2Ph; X = halide, Me, Et, *ansa*-bridge, CF_3)[7–11] and binuclear complexes of the type $[(\eta^5\text{-}(C_5R_5)_2M_2O_5]$ (M = Mo, W)[12,13] have been used as epoxidation catalysts with *tert*-butyl hydroperoxide (TBHP) or H_2O_2 as the oxidant.[13–15] Cyclopentadienyl (Cp) Mo complexes sometimes display activities similar to or even higher than that of the well-examined methyltrioxorhenium (MTO)-H_2O_2 system.[16–20] During the past decade, monomeric CpMo tricarbonyl complexes have been established as suitable precursors for catalytically active molybdenum dioxo or oxo–peroxo complexes, which are formed *in situ* with organic hydroperoxides after oxidative decarbonylation.[21–23] Homogeneous epoxidation activities of CpMo complexes as catalysts have been compared in a recent review[10] and other reviews have discussed heterogenization and catalytic applications of the aforementioned category of molybdenum catalysts.[24–26]

Enantiopure epoxides are valuable in organic synthesis and ubiquitous in pharmaceutical, agrochemical and other fine chemical industrial applications.[27] Numerous molybdenum-based complexes have been utilized in enantioselective catalysis.[28,29] Specifically for epoxidation of unfunctionalized prochiral alkenes, chiral dioxo-molybdenum-based complexes have been extensively studied in both homogeneous and heterogeneous catalysis.[28,30] However, the limited enantioselectivity achieved with such complexes is, in general, a consequence of either weakly coordinating chiral ligands or transition states that are symmetrical during oxygen transfer from the oxo–bisperoxo species.[31] Although stereoselective epoxidation in the homogeneous phase with readily available

Chair of Inorganic Chemistry/Molecular Catalysis, Catalysis Research Center and Department of Chemistry, Technische Universität München, D-85747 Garching bei München, Germany. E-mail: fritz.kuehn@ch.tum.de; Fax: +49 89 289 13473; Tel: +49 89 289 13096

† Electronic supplementary information (ESI) available. CCDC 934898–934900. For ESI and crystallographic data in CIF or other electronic format see DOI: 10.1039/c4cy00738g

Mo catalysts is a lucrative target, only very few examples are reported in the literature and the enantiomeric excess (ee) does not exceed *ca.* 20% (for *trans*-β-methylstyrene as the substrate).[32] Efforts towards the synthesis of chiral CpMo catalysts mostly involve the introduction of chiral substituents on the Cp ring.[32,33] However, as a consequence of the fast rotation of the Cp ring in solution, chiral information is lost, and hence, the ee obtained is very poor. The rotation of the chiral Cp ligand can be suppressed by an *ansa*-bridge from the Cp ligand to the Mo centre that is coordinated either in a heteroatomic fashion[14] or may be σ-C bound.[34] In these cases, the chiral centres are located either at the *ansa*-bridge directly or at substituents at the bridge, which is apparently too far away from the metal to be able to effectively transfer chiral information to the substrate. Royo *et al.* have investigated a chiral oxazoline-substituted Cp molybdenum complex, which forms a heteroatomic *ansa*-bridge in order to introduce chiral centres in close proximity to the metal centre.[14] However, the oxazoline moiety decoordinates and loss of the Cp ligand during catalysis occurs. Hence, the efficiency of stereoselectivity in catalytic epoxidation with $[CpMo(CO)_3X]$ precatalysts also depends on the strength of the Mo–X bond.

In view of the strategic importance of enantiopure epoxides in many industrial endeavors and the efficiency of CpMo complexes in achiral epoxidation,[10] complexes **1–5** have been synthesized (Scheme 1). The ligands utilized are alkyl moieties of the type $–CHR^2–COOR^1$ (R^1 = ethyl (**1**), menthyl (**4**), and bornyl (**5**), R^2 = H; R^1 = ethyl, R^2 = methyl (**2**) and phenyl (**3**)) where the chiral information is located at the R^1 group in complexes **4** and **5**. Compared to the inductive effect of the chloro (electron-withdrawing) and the methyl (electron-donating) group in complexes $[CpMo(CO)_3Cl]$ and $[CpMo(CO)_3Me]$, respectively, the alkyl ester group renders the metal centre more electron poor than the methyl substituent but less than the chloro substituent since the electron-withdrawing ester group is not directly bound to the metal. This is useful for verifying ligand effects on the Lewis acidity of the metal centre in the precatalyst and establishing a correlation with catalytic activity in the epoxidation reaction. Furthermore, complexes **1–5** are designed to be less active than the chloro and methyl analogues and thus may allow for better thermodynamic and kinetic control during enantioselective epoxidation as well as *in situ* monitoring of the catalyzed reaction. The presence of the alkyl ester moiety also eliminates the possibility of β-hydrogen elimination decomposition processes, which are possible for complexes where molybdenum is attached to a large alkyl group.[35]

In this work, the synthesis, characterization and applications of CpMo complexes **1–5** for epoxidation of unfunctionalized olefins such as *cis*-cyclooctene, 1-octene, *trans*- and *cis*-stilbene and *trans*-β-methylstyrene with TBHP as the oxidant are reported. In addition, the progress of catalytic epoxidation of *cis*-cyclooctene has been monitored by ^1H and ^{13}C NMR spectroscopy in order to confirm that the chiral side chain remains coordinated during catalysis.

Experimental

Methods and materials

$[Mo(CO)_6]$, NaH (60% dispersion in mineral oil), ethyl chloroacetate, ethyl lactate, ethyl mandelate, (–)-borneol, (–)-menthol, *tert*-butyl hydroperoxide (TBHP, ~5.5 M solution in *n*-decane), and *trans*-β-methylstyrene were purchased from Sigma Aldrich. All manipulations involving air-sensitive materials were performed under an argon atmosphere using standard Schlenk techniques and dry solvents. Menthyl and bornyl chloroacetate ligands were synthesized by the reaction of L-(–)-menthol and (–)-borneol with chloroacetyl chloride and *N*,*N*-dimethylamine at 0–30 °C. Ethyl lactate mesylate and ethyl mandelate mesylate were also obtained by reaction with mesyl chloride in toluene.[36] Ethyl chloroacetate was degassed and dried by the freeze–pump–thaw method and ethyl lactate mesylate and ethyl mandelate mesylate were distilled at low pressures prior to use for the synthesis of complexes **1–5**. High-resolution NMR spectra were recorded using a Bruker Avance DPX-400 spectrometer. ^1H and ^{13}C spectra are referenced to solvent residual signals[37] and ^{95}Mo spectra to an internal standard of 2 M Na_2MoO_4 in D_2O set at 0 ppm. Solid-state NMR spectra were recorded using a Bruker Avance 300 spectrometer at room temperature in a 4-mm ZrO_2 rotor at 10 kHz or 12 kHz. Adamantane was used as an external (secondary) standard for referencing TMS (^1H: 2.00 ppm, ^{13}C: 29.472 ppm). IR spectra were recorded using a Varian ATR-FTIR instrument. Thermogravimetric analyses were performed with a Netzsch TG 209 system at a heating rate of 10 °C min^{-1} under argon. Microanalyses were performed in the Mikroanalytisches Labor of the Technische Universität München, Garching. Mass spectra were recorded with Finnigan MAT 311

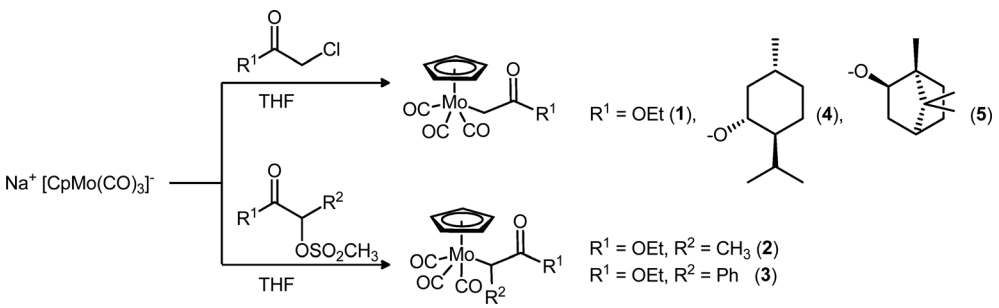

Scheme 1 Synthesis of cyclopentadienyl molybdenum tricarbonyl alkyl ester complexes **1–5**.

A and MAT 90 spectrometers. Catalysis was performed under an ambient atmosphere and catalytic runs were monitored using a Varian CP-3800 instrument equipped with an FID, an Optima 5 Amine column (*cis*-cyclooctene, 1-octene, *trans*- and *cis*-stilbene) and an Optima Delta Amine column (*trans*-β-methylstyrene).

X-ray crystallography

Data were collected using a single-crystal X-ray diffractometer equipped with a CCD detector (APEX II, κ-CCD), a rotating anode (Bruker AXS, FR591) with MoK_α radiation (λ = 0.71073 Å) and a graphite monochromator. Depending on the complex, either a Montel-type focusing optic (compound **2**) or a fine-focus sealed tube (compounds **1** and **5**) was used. Collected data were analyzed by using the SMART software package.[38] The measurements were performed on single crystals coated with perfluorinated ether. The crystals were fixed on top of a glass fiber and transferred to the diffractometer. The crystals were frozen under a stream of cold nitrogen. A matrix scan was used to determine the initial lattice parameters. Reflections were merged and corrected for Lorenz and polarization effects, scan speed, and background using SAINT.[39] Absorption corrections including odd- and even-ordered spherical harmonics were performed using SADABS.[39] Space group assignments were based on systematic absences, *E* statistics, and successful refinement of the structures. Structures were solved by direct methods with the aid of successive difference Fourier maps and refined against all data using the APEX 2 software[38,40] in conjunction with SHELXL-97[41] and SHELXLE.[42] Unless otherwise stated, methyl hydrogen atoms were refined as a part of rigid rotating groups with a C–H distance of 0.98 Å and $U_{iso(H)} = 1.5 \times U_{eq(C)}$. Other H atoms were placed in calculated positions and refined using a riding model with methylene and aromatic C–H distances of 0.99 and 0.95 Å, respectively, and $U_{iso(H)} = 1.2 \times U_{eq(C)}$. If not mentioned otherwise, non-hydrogen atoms were refined with anisotropic displacement parameters. Full-matrix least-squares refinements were carried out by minimizing $\sum w(F_o^2 - F_c^2)^2$ with the SHELXL-97[41] weighting scheme. Neutral atom scattering factors for all atoms and anomalous dispersion corrections for non-hydrogen atoms were taken from the *International Tables for Crystallography*.[43] Images of the crystal structures were generated by PLATON.[44] Full refinement was straightforward for complex **1**, while the ethyl moieties in **2** were refined using split-layer positions. Due to physically meaningless ADPs, the following restraints were applied: SIMU for C1 > C5 (Cp moiety) and ISOR for C10 of complex **5**.

Crystallographic data (excluding structure factors) for the structures have been deposited in the Cambridge Crystallographic Data Centre as supplementary publication no. CCDC-934898 (**1**), CCDC-934899 (**2**) and CCDC-934900 (**5**).

General procedure for synthesis of 1–5

$Na[CpMo(CO)_3]$ (1 equiv.) was prepared by refluxing $Mo(CO)_6$ and NaCp in freshly distilled, dry THF overnight. The yellow-orange oily residue obtained after removing THF *in vacuo* was purified by washing with cold, dry Et_2O (3 × 10 mL). 40 mL of dry THF was then added followed by dropwise addition of a degassed solution of a chloro or a mesylate reagent (1.05 equiv.) in 10 mL of THF under steady argon flow in the dark at −40 °C. The reaction flask was stirred at r.t. in the dark for a suitable time followed by evaporation of the solvent to dryness. The obtained residues were extracted with dry pentane or hexane and concentrated under vacuum. The red-yellow products were then purified by column chromatography (SiO_2). Complexes **1–5** eluted as yellow bands after a deep red band of $Cp_2Mo_2(CO)_6$ using *n*-pentane : diethyl ether = 9 : 1. The fractions were concentrated under vacuum and **1–5** were obtained as yellow solids/oil in yields 54–85%.

$CpMo(CO)_3(CH_2COOC_2H_5)$ (1). Reaction time = 6 h, yield = 73%. Bright yellow solid. ^{1}H NMR (400 MHz, C_6D_6) δ 4.62 (s, 4H, Cp), 4.07 (q, J = 7.1 Hz, 2H), 1.88 (s, 2H, Mo–CH_2), 1.11 (t, J = 7.1 Hz, 3H). $^{13}C\{^1H\}$ NMR (101 MHz, C_6D_6) δ 240.63, 226.99 (Mo–*C*O), 181.07 (*C*=O), 93.44 (Cp), 59.37 (COO*C*H_2CH$_3$), 14.74 (COOCH$_2$*C*H$_3$), −3.77 (Mo–*C*H_2). ^{95}Mo (C_6D_6) = δ −1546. Elemental analysis calcd. (%): C 43.39, H 3.64; found: C 43.56, H 3.70. IR (cm^{-1}, C_6D_6) 2026 *s* (Mo–CO), 1926 *vs.* (Mo–CO), 1682 *w* (ester C=O).

$CpMo(CO)_3(CH(CH_3)COOC_2H_5)$ (2). Reaction time = 24 h, yield = 54%. Yellow solid. ^{1}H NMR (400 MHz, C_6D_6) δ 4.63 (s, 5H, Cp), 4.05 (q, 2H), 2.90 (d, J = 7.1 Hz, 1H, Mo–C*H*), 1.61 (d, J = 7.1 Hz, 3H, Mo–CH–CH_3), 1.11 (t, J = 7.1 Hz, 3H). $^{13}C\{^1H\}$ NMR (101 MHz, C_6D_6) δ 241.00, 228.28, 227.63 (Mo–*C*O), 182.63 (C=O), 93.90 (Cp), 59.33 (COO*C*H_2CH$_3$), 23.61 (Mo–*C*H), 14.68 (COOCH$_2$*C*H$_3$), 11.32 (Mo–CH–*C*H$_3$). ^{95}Mo (C_6D_6) = δ −1484. Elemental analysis calcd. (%): C 45.10, H 4.08, Mo 27.71; found: C 45.72, H 4.23, Mo 25.65. IR (cm^{-1}, C_6D_6) 2010 *s* (Mo–CO), 1914 *vs.* (Mo–CO), 1666 *vs.* (ester C=O).

$CpMo(CO)_3(CH(Ph)COOC_2H_5)$ (3). Reaction time = 48 h, yield = 65%. Yellow solid. ^{1}H NMR (400 MHz, C_6D_6) δ 7.63 (d, J = 7.3 Hz, 2H), 7.15 (m, 2H), 6.95 (t, J = 7.3 Hz, 1H), 4.48 (s, 5H, Cp), 4.15 (s, 1H, Mo–C*H*), 4.04 (m, 2H), 1.08 (t, 3 H). $^{13}C\{^1H\}$ NMR (101 MHz, C_6D_6) δ 241.35, 228.81, 228.72 (Mo–CO), 178.80 (C=O), 147.97 (MoCH(COOEt)*C* (phenyl)), 128.15, 124.74 (phenyl ring C, one signal not clearly observed due to C_6D_6 solvent residual peaks in the same region), 94.82 (Cp), 59.53 (COO*C*H_2CH$_3$), 21.39 (Mo–*C*H), 14.53 (COOCH$_2$*C*H$_3$). ^{95}Mo (C_6D_6) = δ −1515. Elemental analysis calcd. (%): C 52.96, H 3.95, Mo 23.50; found: C 54.10, H 4.06, Mo 22.43. IR (cm^{-1}, C_6D_6) 2023 *s* (Mo–CO), 1930 *vs.* (Mo–CO), 1689 *w* (ester C=O).

$CpMo(CO)_3(CH_2COOMenthyl)$ (4). Reaction time = 12 h, yield = 70%. Bright yellow oil. ^{1}H NMR (400 MHz, C_6D_6) δ 4.85–4.95 (m, 1H), 4.7 (s, 4H, Cp), 2.1–2.3 (m, 2H), 1.84–1.97 (m, 2H), 1.41–1.60 (m, 3H), 1.20–1.38 (m, 1H), 1.07–1.09 (m, 1H), 0.89–1.04 (m, 10H), 0.67–0.8 (m, 1H). $^{13}C\{^1H\}$ NMR (101 MHz, C_6D_6) δ 240.72, 226.91, 226.77 (Mo–*C*O), 180.71 (C=O), 93.44 (Cp), 73.00 (MoCH$_2$(CO)O*C**H(menthyl)), 47.78 (CH$_2$*C*(^{i}Pr)C*HO–(CO)–CH$_2$Mo), 41.89 (CH(Me)*C*H$_2$C*HO–(CO)–CH$_2$Mo), 34.65 (C(^{i}Pr)CH$_2$*C*H$_2$CH(Me)), 31.75 (CH$_2$–*C*H(Me)–CH$_2$–),

26.65 (*C*H(CH_3)$_2$), 23.82 (C(^{i}Pr)*C*$H_2$$CH_2$CH(Me)), 22.43, 21.16, 16.76 (CH_3 groups (menthyl)), −3.36 (Mo–*C*H_2). ^{95}Mo (C_6D_6) = δ −1553. Elemental analysis calcd. (%): C 54.30, H 5.92, Mo 21.69; found: C 55.36, H 6.28, Mo 21.85. IR (cm^{-1}, C_6D_6) 2028 *s* (Mo–CO), 1934 *vs.* (Mo–CO), 1679 *w* (ester C═O).

CpMo(CO)$_3$(CH_2COOBornyl) (5). Reaction time = 12 h, yield = 85%. Yellow solid. ^{1}H NMR (400 MHz, C_6D_6) δ 5.13–5.17 (m, 1H), 4.66 (s, 4H, Cp), 2.42–2.55 (m, 1H), 2.28–2.38 (m, 1H), 1.88–2.01 (m, 2H), 1.66–1.80 (m, 1H), 1.53–1.60 (m, 1H), 1.30–1.47 (m, 2H), 1.14–1.24 (m, 1H), 0.70–1.01 (m, 9H), 0.43–0.55 (m, 1H). ^{13}C{^{1}H} NMR (101 MHz, C_6D_6) δ 240.58, 227.00, 226.85 (Mo–*C*O), 181.48 (C═O), 93.53 (Cp), 79.27 (Mo–CH_2(CO)O*C**H(bornyl)), 48.91, 48.04, 45.40 (bridgehead quaternary C of the bornyl moiety), 37.54, 28.56, 27.74 (–*C*H_2– (bornyl)), 19.92, 18.99, 13.98 (CH_3 groups (bornyl)), −3.35 (Mo–*C*H_2). ^{95}Mo (C_6D_6) δ −1555. Elemental analysis calcd. (%): C 54.55, H 5.49, Mo 21.79; found: C 54.81, H 5.62, Mo 21.91. IR (cm^{-1}, C_6D_6) 2023 *s* (Mo–CO), 1931 *vs.* (Mo–CO), 1669 *s* (ester C═O).

Epoxidation catalysis

All catalytic investigations were carried out under air either in CH_2Cl_2, under solvent-free conditions (22 °C) or in $CHCl_3$ (55 °C). Under standardized conditions, 1 mol% or 0.1 mol% catalyst and the substrate were dissolved in 5 mL of solvent. Catalysis was started with the addition of TBHP to the catalyst and substrate reaction mixture. Aliquots were obtained from the reaction flask at suitable time intervals and treated with activated MnO_2 to destroy the oxidant followed by filtration through a $MgSO_4$ plug to remove traces of water. Appropriate amounts of external standard solutions (indane and *p*-xylene for *cis*-cyclooctene, toluene and mesitylene for 1-octene, hexadecane and octadecane for *cis*- and *trans*-stilbene, 1,2,4-trimethylbenzene and tetraline for *trans*-β-methylstyrene in isopropanol) were then added to the aliquot. The sample was injected into a GC-MS instrument with a column pre-calibrated with r^2 = 0.999 to the chosen substrate. Enantiomeric excess (ee) was calculated from the integration of the two peaks relative to the calibration method optimized with pure sample injections of (2*S*,3*S*)-2-methyl-3-phenyloxirane and (2*R*,3*R*)-2-methyl-3-phenyloxirane.

Typical reaction conditions and data acquisition for NMR study of catalytic epoxidation

For catalytic epoxidation of *cis*-cyclooctene, a mixture of *ca.* 0.1 mmol of **5** and a known amount of mesitylene was dissolved in 0.4 mL of $CDCl_3$ in an NMR tube and its ^{1}H and ^{13}C spectra were recorded. 10 equiv. of *cis*-cyclooctene was then added to the NMR tube and after mixing properly, ^{1}H and ^{13}C NMR were measured. Subsequently, 20 equiv. of TBHP (5.5 M *n*-decane solution) was added at 22 °C and mixed with the precatalyst and substrate solution. It was necessary to shim the magnet again after addition of TBHP for field locking. Using the *multizg* acquisition program of a Bruker© TopSpin spectrometer, data collection could be automated. The ^{1}H spectrum (16 scans (~1.5 min)) was first recorded at 5 min after addition of TBHP followed by the ^{13}C spectrum (164 scans (~8.5 min)). Thus, in an alternating manner, ^{1}H and ^{13}C spectra were collected at 10-minute intervals for a total time of 4 h.

Data analysis for ^{1}H NMR experiments: using NMR software MestReNova©, the characteristic signal of the internal standard mesitylene centred at 6.65 ppm was integrated to 3 H in all ^{1}H NMR spectra. The concentration of oxidized species in each spectrum was then determined by the integral of the Cp signal with correlation for 5 H.

Results and discussion

Synthesis and characterization of complexes 1–5

Complexes **1–5** were synthesized in yields of 54–85% by procedures analogous to previous reports for the synthesis of complex **1**[45,46] using Na[CpMo(CO)$_3$] as the metal precursor and either α-chloroesters (complexes **1**, **4** and **5**) or α-methanesulfonoxyesters (for **2** and **3**) as alkylating agents (Scheme 1).[47]

Complexes **1–3** and **5** are yellow solids and complex **4** is obtained as a bright yellow oil after column purification. All complexes are soluble in benzene, toluene, tetrahydrofuran and dichloromethane. In the solid state, they are stable in air and moisture for several hours, but in solution, they are significantly more sensitive and show visible decomposition associated with a colour change from yellow to blue-green and formation of blue residues overnight. Compounds **1–5** can be handled briefly under ambient conditions without any apparent decomposition, but similar complexes are known to be susceptible to either slow photochemical transformation in solution to μ-CO-bridged species[48] or rearrangement to the η^3-coordinated side chain on the loss of a carbonyl ligand.[49] Complexes similar to **2** are known to be susceptible to β-hydrogen elimination[50] but in the case described here, decomposition of **2** to an α-alkenyl type of complex was not observed. These complexes are stable for over a year when stored in the dark under argon at −30 °C. While complexes **2** and **3** decompose at 150 °C and 110 °C, respectively, Mo complexes **4** and **5** bearing menthyl and bornyl moieties decompose at 210 °C and 205 °C, respectively, as shown by TGA-MS measurements. Although elemental analyses of complexes **2**, **3** and **4** give poor results, solution ^{1}H, ^{13}C and ^{95}Mo NMR and mass spectra (see the ESI†) do not indicate any impurities. Formation of Mo oxides is a possibility under combustion analysis conditions, which is a probable cause for deviation from calculated results.

NMR spectroscopy

^{1}H NMR spectra of compounds **1–5** (in C_6D_6) show the C_5H_5 ligand in the range 4.48–4.70 ppm and 93.44–94.82 ppm in ^{13}C NMR (Table 1). These chemical shift values for the Cp ligand are in the range observed for other structurally similar [CpMo(CO)$_3$X] complexes (where X = Cl and CH_3). The deshielding effect of the ester group on Mo–CH_2 protons is

Table 1 Selected NMR spectroscopic data for complexes **1**–**5** and comparison with [CpMo(CO)$_3$Cl] and [CpMo(CO)$_3$CH$_3$]

	^{1}H^a		^{13}C{^{1}H}^{a}				
Complex	Cp	Mo–$^{\alpha}$C*H*	Cp	Mo–$^{\alpha}$*C*H	*C*(=O)O	Mo–*C*≡O	^{95}Mo^c
1^b	4.68	1.84 (s, 2H)	—	−3.94	—	227.04, 240.63	—
1	4.62	1.88 (s, 2H)	93.44	−3.78	181.05	226.99, 240.63	−1546
2	4.63	2.87–2.93 (q, 1H)	93.90	23.61	182.63	227.63, 228.28, 241.00	−1484
3	4.48	4.15 (s, 1H)	94.82	21.39	178.80	228.72, 228.81, 241.35	−1349
4	4.70	2.16 (m, 2H)	93.44	−3.36	180.71	226.77, 226.91, 240.72	−1553
5	4.66	1.93 (m, 2H)	93.53	−3.35	181.48	226.85, 227.00, 240.58	−1555
[CpMo(CO)$_3$Cl]	4.62	—	95.58	—	—	225.21, 242.99	−887
[CpMo(CO)$_3$CH$_3$]	4.42	0.39	92.41	1.44	—	227.37, 240.49	−1736

^{a} All signals are referenced to deuterated solvent C_6D_6 δ 7.16 (for ^{1}H) and δ 128.06 (for ^{13}C{^{1}H}). ^{b} Ref. 45. ^{c} All signals are referenced to 2 M Na_2MoO_4 in D_2O set at 0 ppm.

partly offset by the metal centre, which is coordinated to three backbonding CO ligands, and therefore, these protons appear upfield (1.88–2.16 ppm) for **1**, **4** and **5**. On the other hand, the Mo–$^{\alpha}$C*H* signals of **2** and **3** are highly deshielded, appearing downfield at 2.90 and 4.15 ppm, respectively. This deshielding is also reflected in the respective ^{13}C NMR shifts of the α-carbon observed at 21.39 and 23.61 ppm for complexes **2** and **3**, respectively, in contrast to the highly upfield Mo–$^{\alpha}$*C*H$_2$ signals ranging from −3.35 to −3.78 ppm for **1**, **4** and **5**.

In ^{13}C NMR spectra, the carbonyl resonances of complexes **2**–**5** (in C_6D_6) appear as three well-resolved peaks, one each for the two *syn* carbonyls and one for the third *trans* carbonyl known to appear downfield to the two *cis* CO.[51] Similar to [CpMo(CO)$_3$X] complexes (X = Me and Cl), compound **1** shows no such inequivalence in the chemical shift for the terminal carbonyl groups and only two signals are observed.

Variable temperature ^{13}C NMR studies of **5** in C_6D_6 demonstrate that the stereoelectronic asymmetry observed in the form of two suitably resolved peaks for the electronically inequivalent '*cis*-CO' is present even until 70 °C. Coalescence of the two carbonyl signals does not occur even at this high temperature (Fig. S6, ESI†). Solid-state ^{1}H MAS and ^{13}C CPMAS NMR spectra of **5** have been compared to those of [CpMo(CO)$_3$Me] (Fig. S7, ESI†). For complex **5**, all three Mo-bound carbonyl groups show chemical shift anisotropy in the solid state and appear at 226.59, 230.16 and 242.25 ppm, in contrast to [CpMo(CO)$_3$Me] where the two *cis*-CO are equivalent at 230.3 ppm and the third appears at 242.3 ppm. This suggests that the possible fluxional processes, namely, rotation of Cp about the Mo-(η^5-Cp) C_5 axis, rapid interchangeability equivalence of the square pyramidal basal *cis*-CO ligands, rotation about the Mo–αC σ bond, and Berry-type pseudorotation[52–56] might be slower or restricted probably due to the presence of bulky substituents in compounds **2**–**5**. However, for the [CpMo(CO)$_3$Me] complex, no such inequivalence is apparent and only two carbonyl peaks can be observed in solution and solid-state ^{13}C NMR spectra. Complexes **2**–**5** are thus examples of monomeric cyclopentadienyl tricarbonyl molybdenum piano-stool complexes where the barriers to various fluxional processes involving Cp and basal ligands are significant even at high temperatures. It is worth noting that the solution NMR spectra of complexes **4** and **5** and the X-ray structure of **5** (Flack parameter 0.02(7), see the ESI†) confirm the enantiopurity of the prepared complexes.

^{95}Mo NMR chemical shifts are regarded as a suitable indicator of the electronic situation or the Lewis acidity of the metal centre.[57] The ^{95}Mo chemical shifts of complexes **1**, **4** and **5** are similar, seen at *ca.* −1550 ppm. For complexes **2** and **3**, the chemical shifts are observed at −1484 ppm and −1349 ppm, respectively. These lie in between the ^{95}Mo shift of known tricarbonyl complexes [CpMo(CO)$_3$Cl] (at −887 ppm) and [CpMo(CO)$_3$CH$_3$] (at −1736 ppm). The trend in chemical shifts (–Cl compared to the –CH$_3$ complex) can be interpreted to indicate that an electron-withdrawing substituent at the Mo centre shows a downfield shift in comparison with an electron-donating group.[57] This implies that the Mo centre is more electron-deficient in compound **3** compared to that in complex **2**, which is in agreement with the expected substituent effects (–CH$_3$ *vs.* –C$_6$H$_5$ at α-C in conjunction with the ester functional group).

Vibrational spectroscopy

The carbonyl ester group in **1**–**5** absorbs in the range of 1666–1690 cm^{-1}, which is typical for complexes of this type.[46] The absorption frequencies for the terminal carbonyl groups differ only about 15 cm^{-1} in **1**–**5**. The chemical shift anisotropy, which is observed in solution and solid-state NMR spectra of metal-bound carbonyl groups, is not clearly evident in the absorption pattern and only two bands are seen in the range of 2023–2028 cm^{-1} and 1926–1931 cm^{-1}.[58] This is not altogether unusual as deviation from the original D_{4h} geometry to the slightly perturbed C_{3v} geometry in piano-stool complexes results in experimental observation of only two bands, A′ and A″, out of the three possible ν_{CO}.

Thermogravimetry and mass spectrometry

Thermogravimetric analysis combined with mass spectrometry data for complexes **2**–**5** indicate that the loss of a Mo-bound carbonyl group (as CO$^+$) initiates their decomposition. This is followed by a nearly simultaneous loss of Cp, the other two carbonyls or the alkyl ester side chain. These transformations are responsible for the complete

decomposition of the precatalysts. The propensity of both processes is accentuated when one CO is lost. Mass spectrometry and decomposition points determined from TGA-MS are given in Table 2.

Single-crystal X-ray diffraction

Crystals of complexes **1**, **2** and **5** were obtained from a pentane–diethyl ether solvent mixture by slow vapor diffusion and were suitable for single-crystal X-ray diffraction experiments. The crystal structures of these complexes prove indisputably the η^1-coordination of the ester side chain (Fig. 1–3).

The bond length Mo1–C9 (Mo–$^{\alpha}$C) in the crystal structures of complexes **1**, **2** and **5** differs significantly. This bond distance is the shortest for complex **1** (2.325(2) Å) due to the least steric demand in the absence of any α-C substituent, while in complex **2** (2.377(2) Å), the presence of the methyl substituent exerts a higher steric demand and thus the bond length increases. For complex **5**, the bond length Mo1–C9 is 2.349(5) Å, which is in between those for **1** and **2**. Here, the steric influence is a result of the bulky bornyl ester group even though there is no additional α-C substituent. The Mo–$^{\alpha}$C bond length in complex [$CpMo(CO)_3CH_3$] is 2.326(3) Å,[59] which is almost identical to the bond length in complex **1**.

All terminal Mo–CO bonds and C–O bond lengths for **1**, **2** and **5** are equal (within statistical error) and lie in the expected range. Furthermore, the bond angle Cp–Mo1–C9 is smaller for complex **1** (109.01(6)°) when compared to those for complexes **2** and **5** (110.71(6)° and 111.0(2)°, respectively). The torsion angle Cp–Mo1–C9–C10 is −177.8(2)° in **1**, −59.8(2)° in **2** and −51.2(4)° in **5**, which indicates that the alkyl ester moiety can rotate freely in **2** and **5** but only a staggered conformation of Cp–Mo1–C9–C10 is possible in complex **1**. In addition, the torsion angle C7–Mo1–C9 differs in the three complexes significantly. It has the highest value for **1** (136.2(1)°), which is possibly a consequence of conformation or packing effects, while in complexes **2** (134.4(1)°) and **5** (132.7(3)°), the higher steric demand and the *gauche* conformation to Mo1–Cp make a close proximity between C9 and CO ligands possible, making the torsion angle smaller than that for **1**.

Epoxidation catalysis

All complexes were applied as catalyst precursors for the epoxidation of *cis*-cyclooctene and 1-octene as well as the prochiral olefins *trans*- and *cis*-stilbene and *trans*-β-methylstyrene with TBHP (5.5 M in *n*-decane) as the oxidant. Different molar ratios of the catalysts, 1 mol% and 0.1 mol%, were investigated and the ratio of substrate : TBHP = 1 : 2 was utilized in all reactions, which were carried out at 22 and 55 °C. Catalytic reactions were investigated under air in 5 mL of solvent dichloromethane, chloroform or in the absence of a solvent. For all catalytic reactions, <1% conversion of all substrates to their epoxides was observed in the absence of the molybdenum precatalyst, and similarly, the oxidant alone without the catalyst was ineffective in any appreciable epoxidation of the chosen substrates. Yield and TOF for each catalytic experiment are given in Tables S1 and S2 in the ESI.†

During catalytic epoxidation of *cis*-cyclooctene with **1**–**5** and TBHP, an induction period is observed that lasts for 30 min to 2 h depending on the catalyst. This initial time period is attributed to oxidative decarbonylation of the Mo(II)

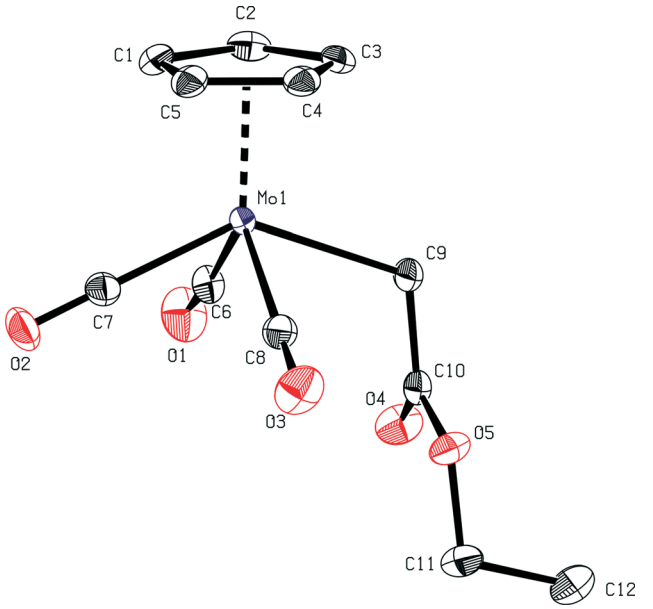

Fig. 1 ORTEP view of the single-crystal X-ray structure of compound **1**. Thermal ellipsoids are drawn at a 50% probability level. Hydrogen atoms are omitted for clarity. Selected bond distances [Å], angles [°] and torsion angles [°]: Mo1–C9 2.325(2), Mo1···Cp 1.9956(2), Mo1–C6 2.002(3), Mo1–C7 1.990(3), Mo1–C8 2.000(3), C6–O1 1.148(4), C7–O2 1.143(3), C8–O3 1.138(4), Cp–Mo1–C9 109.01(6), Mo1–C9–C10 116.0(2), C6–Mo1–C9 77.7(2), C7–Mo1–C9 136.2(1), C8–Mo1–C9 78.4 (2), Mo1–C9–C10–O4 88.1(3), Cp–Mo1–C9–C10 −177.8(2).

Table 2 Mass spectrometry data and decomposition points for complexes **1**–**5**

Complex	MI[a,b]	Base peak	Method[d]	Decomposition point (°C)[e]
1[c]	333	89	CI	32.5–33.5[c]
2	348.6 (14.8)	182.8	CI (+)	150
3	410.5 (13.7)	164.9	CI (+)	110[f]
4	444.6 (4.6)	146.9	FAB (+)	210–220[f]
5	442.5 (19.9)	246.6	FAB (+)	205

[a] % Relative abundance in parenthesis. [b] CI-MS (+) *m*/*z* are M + 1 peaks. [c] Ref. 46. [d] CI refers to chemical ionization; FAB refers to fast atom bombardment method. [e] Determined by TGA-MS under an inert argon atmosphere with Al_2O_3 correction; temperature gradient 10 K min^{-1}. [f] Gradual decomposition, triggered by the loss of one CO^+.

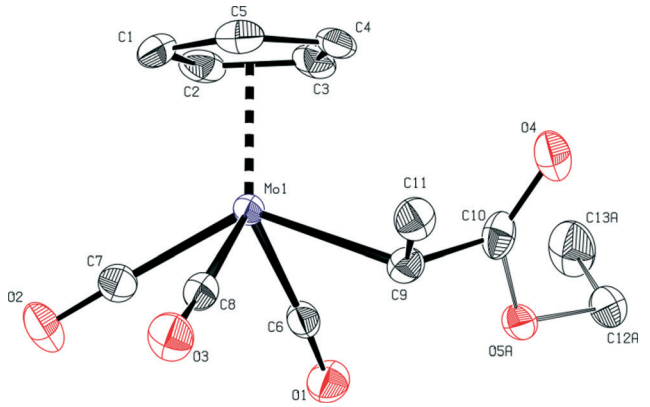

Fig. 2 ORTEP view of the single-crystal X-ray structure of compound **2**. Thermal ellipsoids are drawn at a 50% probability level. The hydrogen atoms and the disorder in the ester moiety are omitted for clarity. Selected bond distances [Å], angles [°] and torsion angles [°]: Mo1–C9 2.377(2), Mo1···Cp 2.0118(3), Mo1–C6 1.997(2), Mo1–C7 1.997(3), Mo1–C8 2.004(2), C6–O1 1.145(3), C7–O2 1.145(3), C8–O3 1.141(3), Cp–Mo1–C9 110.71(6), Mo1–C9–C10 108.3(2), C6–Mo1–C9 78.9(1), C7–Mo1–C9 134.4(1), C8–Mo1–C9 73.6(1), Mo1–C9–C10–O4 96.3(3), Cp–Mo1–C9–C10 −59.8(2).

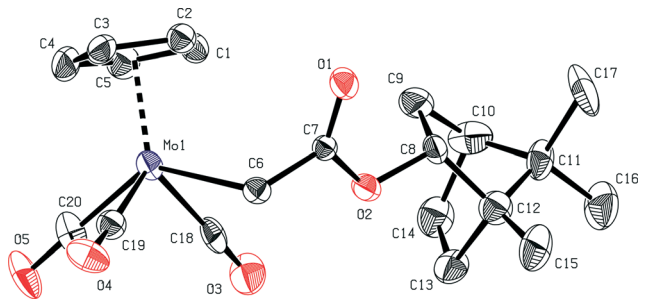

Fig. 3 ORTEP view of the single-crystal X-ray structure of compound **5**. Thermal ellipsoids are drawn at a 50% probability level. Hydrogen atoms are omitted for clarity. Selected bond distances [Å], angles [°] and torsion angles [°]: Mo1–C9 2.349(5), Mo1···Cp 1.9917(5), Mo1–C6 2.008(5), Mo1–C7 1.983(7), Mo1–C8 1.978(7), C6–O1 1.141(6), C7–O2 1.170(8), C8–O3 1.161(7), Cp–Mo1–C9 111.0(2), Mo1–C9–C10 111.0(4), C6–Mo1–C9 77.6(2), C7–Mo1–C9 132.7(3), C8–Mo1–C9 73.5(2), Mo1–C9–C10–O4 91.4(6), Cp–Mo1–C9–C10 −51.2(4).

precatalyst to give the catalytically active oxomolybdenum(VI) species (see Fig. 4 and Scheme 2).[21,22,60] The concentration of active species present in the reaction mixture is very small in the beginning of the reaction, and therefore, conversion of the substrate to its epoxide is originally also small. Once a critical amount of oxidized species is formed, epoxidation of the substrate becomes quite fast, as indicated by the steep part of the plots in Fig. 4.

1–5 are active catalysts for the epoxidation of *cis*-cyclooctene, forming cyclooctene oxide selectively and quantitatively within 2–4 h (1 mol% catalyst) in CH_2Cl_2 (Fig. 4(a)). Activities in the range of 120–190 cycles per hour are observed for cyclooctene oxide formation, which increase to 230–360 h^{-1} when 0.1 mol% of the precatalysts is used (Fig. 4(b)). In the absence of a cosolvent, catalytic epoxidation of *cis*-cyclooctene was accompanied by evolution of heat after the addition of TBHP, indicating that oxidative decarbonylation is exothermic. This is, at least in part, responsible for faster conversions to cyclooctene oxide along with the smaller dilution factor and thus increased TOFs (210–500 h^{-1}) (Fig. 4(c)). At a higher reaction temperature of 55 °C, conversion of *cis*-cyclooctene to its epoxide is very fast and quantitative yields are obtained within 10 min after addition of the oxidant (Fig. 4(d)). There is no clearly discernible induction period for these catalysis experiments and TOFs are 780 h^{-1} (**1**, **4**, **5**), 1020 h^{-1} (**2**) and 1190 h^{-1} (**3**). TOFs for catalytic epoxidation of *cis*-cyclooctene in the case of complexes $[CpMo(CO)_3Cl]$[21] and $[CpMo(CO)_3CH_3]$[11] are 1300 h^{-1} and 820 h^{-1}, respectively, using a catalyst : substrate : TBHP ratio of 1 : 100 : 200 at 55 °C. For catalysis with complexes **2** and **3**, within 5 min of addition of TBHP, rapid evolution of gases is observed with a simultaneous increase in temperature over 55 °C. This temperature increase is a result of oxidative decarbonylation of the tricarbonyl complexes and is responsible for the high activity (as indicated by TOFs) of these complexes. During catalysis with complexes **1**, **4** and **5**, such violent exothermic reactions are not observed; however, due to the high reaction temperature, the conversion of *cis*-cyclooctene is very fast, and for all complexes, quantitative yield of the epoxide is obtained within 15 min.

The stilbene substrates are selectively transformed to their respective epoxides in yields of up to 50% within 4 h and these yields only marginally increase up to 65% after 24 h (Fig. 4(e) and (f)). A more challenging substrate, 1-octene, is converted to its epoxide slowly, and yields of about 40% are obtained after 24 h with 1 mol% of the catalysts. The conversion of the terminal alkene (1-octene) and aromatic substrates (stilbene, methylstyrene) is both poor and slow relative to *cis*-cyclooctene. This can be due to deactivation of the primary catalyst before complete epoxidation of these substrates. There is little influence of the increasing steric bulk of the ester alkyl group from ethyl (**1**, **2** and **3**) to menthyl (**4**) or bornyl (**5**) on catalytic activity, which is not surprising as the electronic situation at the metal centre is similar for the three α-carbon-unsubstituted precatalysts. In addition, the reaction site is farther from the ethyl group or the sterically encumbered menthyl or bornyl groups located at the end of the oxoalkyl side chain.

Although epoxidation of *trans*-β-methylstyrene is selective towards the epoxide product, there is negligible (within the experimental error) stereo-differentiation during catalysis and only equimolar amounts of (2*S*,3*S*)-2-methyl-3-phenyloxirane and (2*R*,3*R*)-2-methyl-3-phenyloxirane are obtained. Poor ee obtained with these complexes can be reasoned to be due to the location of chiral information being still too far away from the reactive metal centre.

Complexes **2** and **3** with a methyl and a phenyl substituent on Mo–$^{\alpha}$C, respectively, are generally more active than complexes **1**, **4**, and **5**, which are unsubstituted at this position. Furthermore, catalysis with **3** gives a slightly higher yield of epoxides for nearly all substrates tested compared to

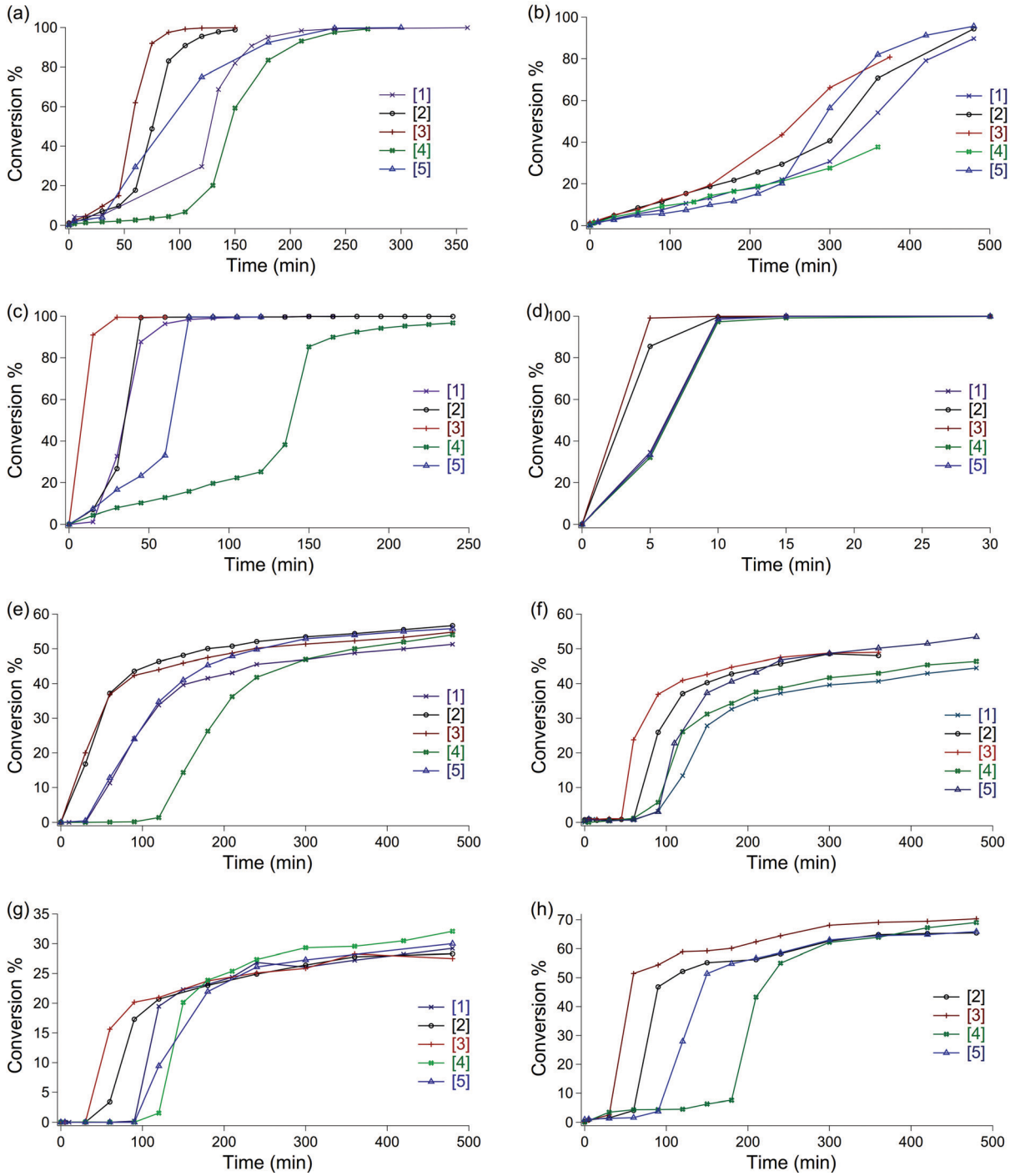

Fig. 4 Conversion *vs.* time plot of different substrates with 1 mol% complexes **1**–**5** and TBHP oxidant at room temperature in dichloromethane unless otherwise stated: (a) *cis*-cyclooctene, (b) *cis*-cyclooctene + 0.1 mol% catalyst, (c) *cis*-cyclooctene, no co-solvent, (d) *cis*-cyclooctene, 55 °C, $CHCl_3$ solvent, (e) *cis*-stilbene, (f) *trans*-stilbene, (g) 1-octene, (h) *trans*-β-methylstyrene. Ratio of catalyst : substrate : oxidant = 1 : 100 : 200.

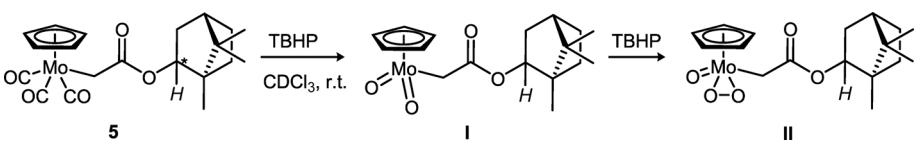

Scheme 2 The oxidation of tricarbonyl precatalyst **5** with 10 equiv. of TBHP (in *n*-decane) results in the formation of both dioxo (**I**) and oxo–peroxo (**II**) species at room temperature in $CDCl_3$.

that with complex **2**. This trend may be accounted for by the observation that the molybdenum centre appears slightly more electron-deficient in **2** and **3** compared to those in precatalysts **1**, **4** and **5**.

NMR study of catalytic epoxidation of *cis*-cyclooctene

In order to confirm the stability of the Mo–R bond in the chiral catalyst during epoxidation, we followed the progress of catalytic epoxidation of *cis*-cyclooctene with TBHP using ^{1}H and ^{13}C NMR. Complex **5** was chosen as the precatalyst since its oxidative transformation is slow enough to be studied on a suitable time scale in NMR at room temperature especially in comparison with precatalysts **2**, **3**, $[CpMo(CO)_3Cl]$ and $[CpMo(CO)_3CH_3]$ for which the reaction was observed to be exothermic. In analogy with previous reports,[9,23] it is proposed that the reaction of **5** with TBHP proceeds as illustrated in Scheme 2, and the oxidized complexes **I** and **II** are the catalytically active species.

A mixture of *ca.* 0.1 mmol of **5** in $CDCl_3$ and 10 equiv. of *cis*-cyclooctene was treated with 20 equiv. of TBHP at 22 °C and the reaction progress was monitored by ^{1}H (Fig. 5) and ^{13}C NMR (Fig. 6). Quantitative epoxidation of *cis*-cyclooctene to its epoxide takes place within 3.5 h, as indicated by the disappearance of the *cis*-cyclooctene multiplet at 5.68–5.85 ppm. However, complex **5** does not undergo complete oxidative decarbonylation and all three terminal CO signals can be observed even after 4 h in ^{13}C NMR (Fig. 6(a)). This indicates that although only a part of the precatalyst is converted to the active species, the rate of epoxidation is quite high. The signal for Cp of precatalyst **5** at 5.22 ppm and a new signal for the oxidized complex at 6.28 ppm can both be observed after 4 h of monitoring the catalysis reaction, confirming that the Cp ligand is retained after the oxidative transformation.

In ^{13}C NMR spectra, a prominent signal from the Cp ligand of the oxidized complex (Cp(ox)) is observed at 111.3 ppm, evolving from the Cp signal at 93.4 ppm of the tricarbonyl precatalyst **5** and has been assigned to the dioxo complex **I**. The proposal outlined in Scheme 2 asserts that *in situ* oxidation of **5** with TBHP forms complexes **I** (dioxo) and (later) **II** (oxo–peroxo) and both are catalytically active for olefin epoxidation. The work presented here supports the possibility of the oxidation shown in Scheme 2 but does not unambiguously support the structures of **I** and **II**. A comparison with NMR data of similar complexes[21] suggests, however, that this assignment is most likely correct. A small signal at 111.7 ppm can be seen (Fig. 6(d)) when the amount of cyclooctene decreases appreciably at later stages of the reaction and has been assigned to the Cp ligand of the oxo–peroxo complex **II** based on the ^{95}Mo NMR chemical shift (see discussion below, Fig. S11 in the ESI†) and crystallographic evidence (Table S3 in the ESI†). Since cyclooctene is converted to its epoxide before the amount of the oxo–peroxo complex is significant, it is evident that the rate of oxidation of olefin with the dioxo complex is quite high. Alternatively, this observation suggests that the presence of the olefin (in its

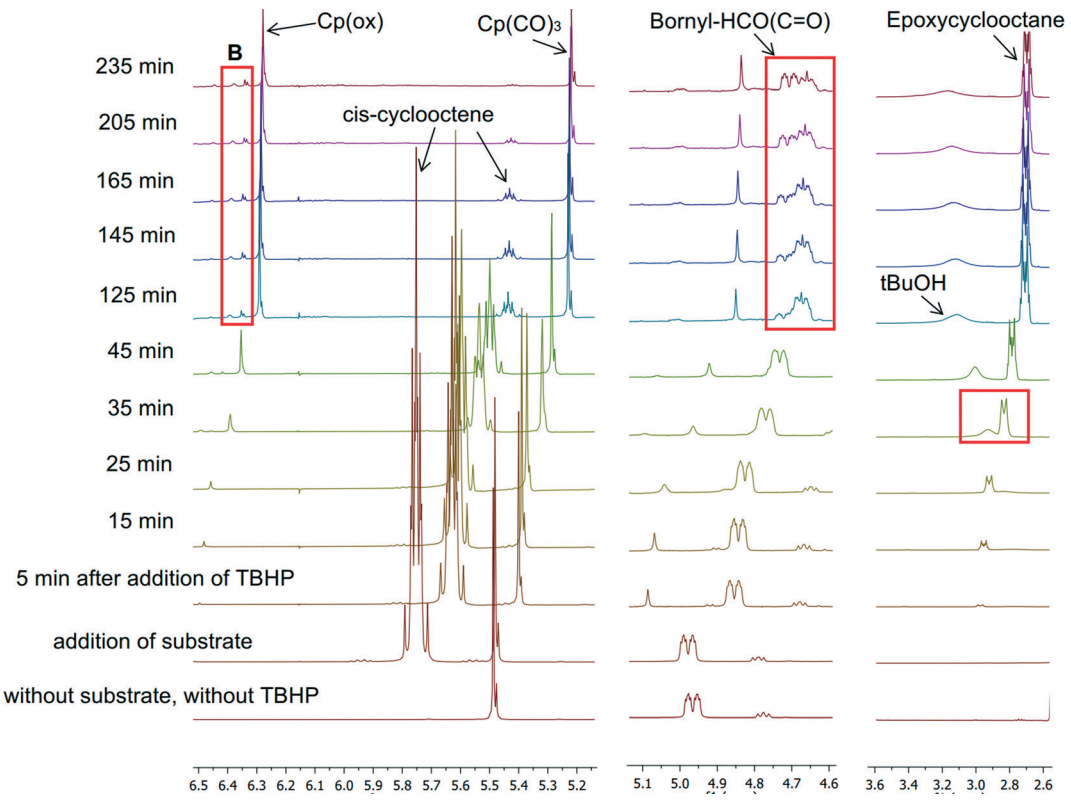

Fig. 5 ^{1}H NMR profile for the reaction of **5** with 10 equiv. of *cis*-cyclooctene and 20 equiv. of TBHP (in decane) in $CDCl_3$ at 22 °C (with mesitylene as the internal standard).

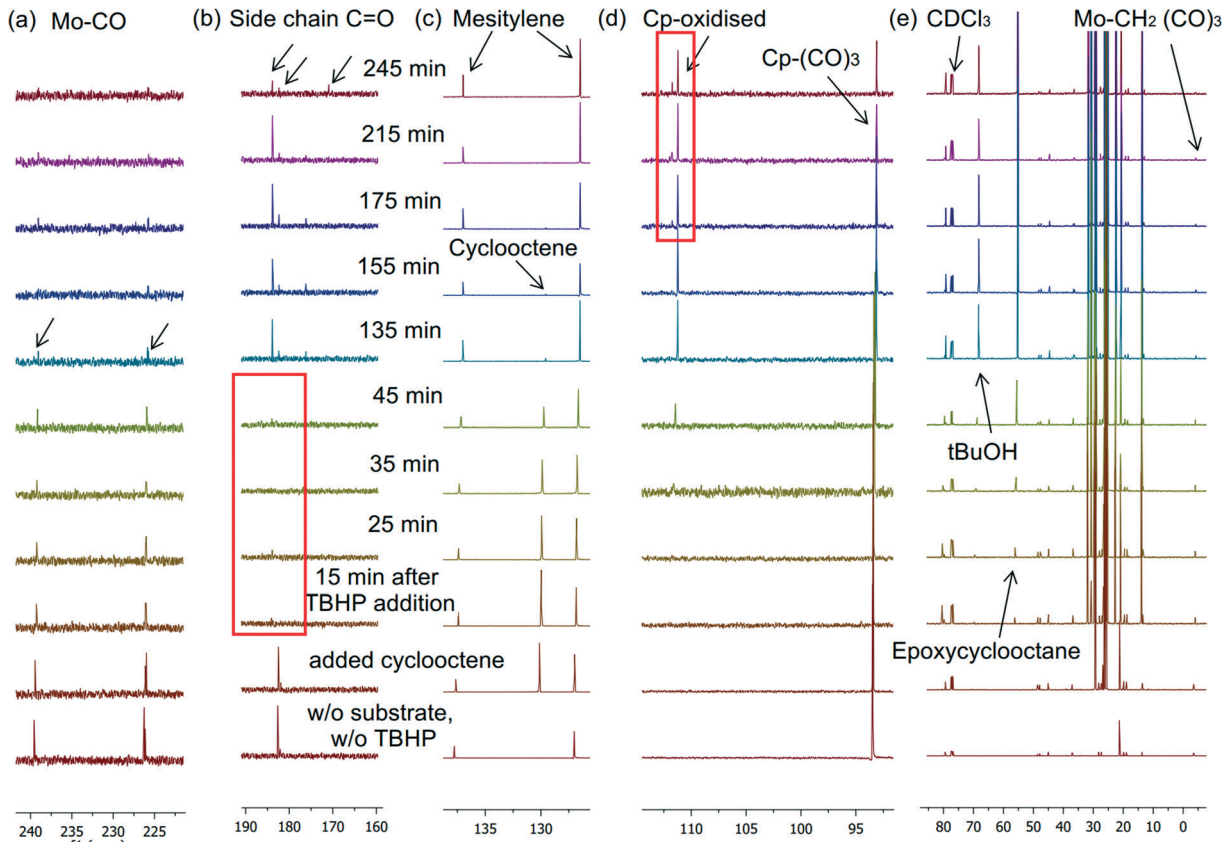

Fig. 6 ^{13}C NMR profile for the reaction of **5** with 10 equiv. of *cis*-cyclooctene and 20 equiv. of TBHP (in *n*-decane) in $CDCl_3$ at 22 °C showing spectral regions for (a) terminal CO, (b) alkylester C═O, (c) mesitylene (internal standard), (d) Cp ligand, and (e) solvent $CDCl_3$, *tert*-butanol, epoxycyclooctane, and alkyl moieties CH_2 and CH_3 of R^1 group in complex **5**.

role as a reductant) affects the oxidation of the precatalyst, *i.e.* by suppressing the conversion of **I** to **II**.

In Fig. 6(b), the signals of the ester carbonyl carbon are not clearly observed in the period following oxidative decarbonylation (between 15 and 45 min) but they reappear at about 55 min. It is unclear why this might occur since the signals of other quaternary carbon (CO group) can still be observed. The chiral side chain does not dissociate during the catalysis reaction, as evident from a persistent multiplet in the ^1H NMR spectrum from 4.6 to 4.76 ppm after 4 h (corresponding to the hydrogen at the bornyl chiral centre from the dioxo complex **I**) and a signal at 170.8 ppm (for the ester carbonyl) in the ^{13}C NMR spectrum. *tert*-Butanol is evolved as a side product, appearing as a broad signal in ^1H spectra from 2.9 to 3.3 ppm. The complete assignment of observed ^1H and ^{13}C NMR chemical shifts is given in Table 3.

The concentration *vs.* time plots illustrated in Fig. 7 follow the progress of catalytic epoxidation and the changes in the concentrations of the substrate, precatalyst **5** and dioxo complex **I**. From a starting concentration of [**5**] = 0.249 M, the amount of **5** present in solution after 3.5 h left unreacted is 0.079 M (31.7%) and the concentration of the catalytically

Table 3 Assignment of ^1H and ^{13}C NMR chemical shifts (in ppm) observed during catalytic epoxidation of *cis*-cyclooctene with **5** and TBHP oxidant in $CDCl_3$ at 22 °C (**5** : CyOc : TBHP = 1 : 10 : 20). R^1 = Bornyl, CyOc = *cis*-cyclooctene, EpCy = epoxycyclooctane

Complex	^1H NMR, δ (ppm)		^{13}C NMR, δ (ppm)		Time
5	Cp	5.22	Cp	93.4	0–4 h
	C(O)OC*H*	4.93–4.99	Mo–*C*O	226.14, 226.36, 239.67	
			(O═*C*)OR^1	182.3 → 184.0[b]	
I	Cp	6.28	Cp	111.3	35 min–4 h
	C(O)OC*H*	4.6–4.76[a]	(O═*C*)OR^1	176.16	
II	Cp	6.27	Cp	111.7[c]	175 min–4 h
	C(O)OC*H*	[a]	(O═*C*)OR^1	171.4[c]	
CyOc	–*H*C═C*H*–	5.68–5.85	–HC═*C*H–	130.0	0–165 min
EpCy	–*H*C–(O)–C*H*–	2.64–2.75	–HC–(O)–*C*H–	55.5	15 min–4 h

[a] See 'Bornyl-*H*C–O–C(O)' in Fig. 5 for changes in the observed multiplet of this proton. [b] Chemical shift changes due to the change in polarity. [c] Observed after 3 h when epoxidation of cyclooctene is complete.

active dioxo species is 0.083 M (~33.3%). This suggests that *in situ* generation of catalytically active complexes is not very efficient. Alternatively, since about one-third of the precatalyst is left unreacted during catalytic epoxidation, these results suggest that the conversion of the cyclooctene substrate to its epoxide takes precedence over a complete oxidative decarbonylation of the precatalyst.

In an attempt to evaluate how such homogeneous catalysts perform in subsequent catalytic runs without isolating the active oxo complex, we added the substrate after treating the precatalyst with TBHP. The ^{95}Mo NMR spectrum of the reaction mixture on treating **5** with 50 equiv. of TBHP in $CDCl_3$ shows a broad signal at −628 ppm (Fig. S11 in the ESI†). This chemical shift is similar to ^{95}Mo signals of other [CpMo(O)(O_2)R] complexes (R = CH_3, −609 ppm; R = CF_3, −709 ppm).[9,23] For this reason, the persistent Cp signal at 6.27 ppm in the ^{1}H NMR spectrum and 111.7 ppm in the ^{13}C NMR spectrum is assigned to the oxidized species (**II**). After 48 h, *cis*-cyclooctene (10 equiv.) was added into the NMR tube containing the pre-oxidized complex (**II**). The concentration of the oxidized complex available for epoxidation of the substrate was determined to be *ca.* 0.054 M. This amount is ~50% less than that present after 4 h of oxidation of the precatalyst (*ca.* 0.11 M), indicating that either **II** is slowly transformed into another species or it undergoes decomposition. Complex **II** also catalyses the transformation of *cis*-cyclooctene to its epoxide, although conversion occurs gradually (Fig. S12 in the ESI†). This may be attributed to the auto-retardation effect of *tert*-butanol, which is present in the reaction mixture after *in situ* oxidation of the precatalyst and/or lower activity of the oxo–peroxo species relative to the dioxo complex.

Accordingly, it can be confirmed that complex **II** (oxo–peroxo) is also an active catalyst for olefin epoxidation.

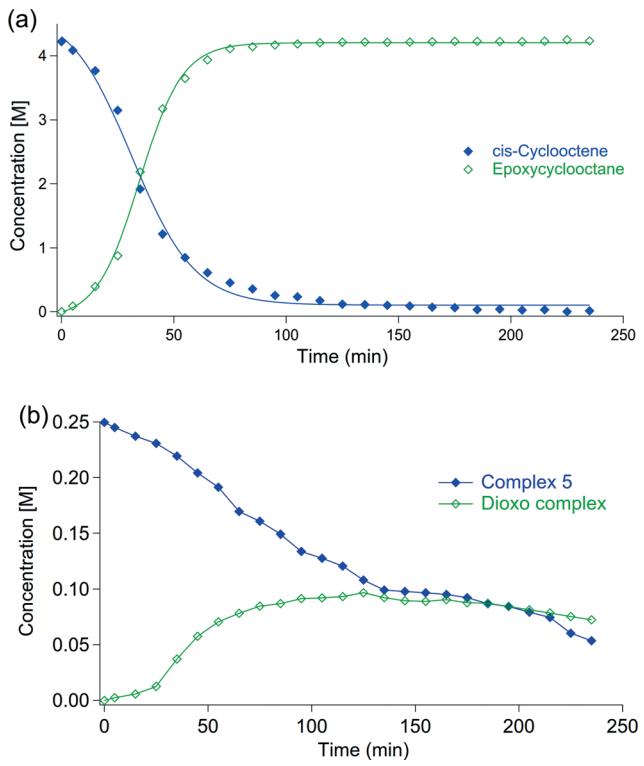

Fig. 7 Concentration *vs.* time plots for (a) catalytic epoxidation of *cis*-cyclooctene with TBHP and (b) the concentration of precatalyst **5** and the catalytically active oxidized complex (**I**) during epoxidation.

Conclusion

Cyclopentadienyl molybdenum complexes with different oxoalkyl side chains have been synthesized and investigated for achiral and chiral epoxidation catalysis. The chiral ligands for the synthesized complexes are derived from cheap and readily available chiral pool compounds. A comparison between substituted and unsubstituted complexes at the α-carbon to molybdenum is presented. The former are more active for the epoxidation of olefins on account of a more electron-deficient metal centre and **3** is a better catalyst for nearly all substrates. **1**–**5** display moderate activities in epoxidation catalysis at room temperature compared to many other half-sandwich tricarbonyl Mo(II) complexes previously reported, and no stereoselectivity is achieved with prochiral substrates, probably due to the pronounced distance between the chiral centres and the catalytic sites. Nevertheless, due to the somewhat reduced catalytic activity, insight into the progress of the precatalyst oxidation and the epoxide formation is gained. Cyclooctene epoxidation progress with precatalyst **5** and TBHP monitored by NMR indicates that *in situ* oxidation of **5** with TBHP forms the highly active dioxo complex, and thus, both the Cp ligand and the chiral side chain are retained. However, *ca.* 32% of precatalyst **5** remain unreacted and catalytic epoxidation takes precedence over complete oxidation of the tricarbonyl precursor. The oxo–peroxo complex is also formed on oxidation of the dioxo complex, albeit only near-complete conversion of the substrate in the epoxidation reaction. The quantitative ^{1}H NMR study also confirms that the oxo–peroxo complex [CpMo(O)(O_2)R] obtained through oxidation of the precursor with TBHP is catalytically active for olefin epoxidation.

Acknowledgements

N.G. is grateful to the TUM Graduate School of Chemistry for financial support.

References

1 *Mechanisms in Homogeneous and Heterogeneous Epoxidation Catalysis*, ed. S. T. Oyama, Elsevier, 2011.
2 S. M. Bruno, B. Monteiro, M. S. Balula, C. Lourenço, A. A. Valente, M. Pillinger, P. Ribeiro-Claro and I. S. Gonçalves, *Molecules*, 2006, **11**, 298–308.
3 A. Günyar and F. E. Kühn, *J. Mol. Catal. A: Chem.*, 2010, **319**, 108–113.

4 A. M. Al-Ajlouni, A. Günyar, M. Zhou, P. N. W. Baxter and F. E. Kühn, *Eur. J. Inorg. Chem.*, 2009, **2009**, 1019–1026.
5 F. E. Kühn, A. M. Santos and M. Abrantes, *Chem. Rev.*, 2006, **106**, 2455–2475.
6 A. Günyar, M.-D. Zhou, M. Drees, P. N. W. Baxter, G. Bassioni, E. Herdtweck and F. E. Kühn, *Dalton Trans.*, 2009, 8746–8754.
7 A. Capapé, A. Raith and F. E. Kühn, *Adv. Synth. Catal.*, 2009, **351**, 66–70.
8 C. Freund, W. A. Herrmann and F. E. Kühn, *Top. Organomet. Chem.*, 2007, **22**, 39–77.
9 S. A. Hauser, M. Cokoja, M. Drees and F. E. Kühn, *J. Mol. Catal. A: Chem.*, 2012, **363–364**, 237–244.
10 N. Grover and F. E. Kühn, *Curr. Org. Chem.*, 2012, **16**, 16–32.
11 J. Zhao, A. M. Santos, E. Herdtweck and F. E. Kühn, *J. Mol. Catal. A: Chem.*, 2004, **222**, 265–271.
12 A. M. Martins, C. C. Romão, M. Abrantes, M. C. Azevedo, J. Cui, A. R. Dias, M. T. Duarte, M. A. Lemos, T. Lourenço and R. Poli, *Organometallics*, 2005, **24**, 2582–2589.
13 C. Dinoi, M. Ciclosi, E. Manoury, L. Maron, L. Perrin and R. Poli, *Chem. – Eur. J.*, 2010, **16**, 9572–9584.
14 P. M. Reis, C. A. Gamelas, J. A. Brito, N. Saffon, M. Gómez and B. Royo, *Eur. J. Inorg. Chem.*, 2011, **2011**, 666–673.
15 V. V. Krishna Mohan Kandepi, J. M. S. Cardoso and B. Royo, *Catal. Lett.*, 2010, **136**, 222–227.
16 T. Michel, M. Cokoja, V. Sieber and F. E. Kühn, *J. Mol. Catal. A: Chem.*, 2012, **358**, 159–165.
17 P. Altmann, M. Cokoja and F. E. Kühn, *Eur. J. Inorg. Chem.*, 2012, **2012**, 3235–3239.
18 T. Michel, D. Betz, M. Cokoja, V. Sieber and F. E. Kühn, *J. Mol. Catal. A: Chem.*, 2011, **340**, 9–14.
19 F. E. Kühn, A. Scherbaum and W. A. Herrmann, *J. Organomet. Chem.*, 2004, **689**, 4149–4164.
20 F. E. Kühn, A. M. Santos and W. A. Herrmann, *Dalton Trans.*, 2005, 2483–2491.
21 M. Abrantes, A. M. Santos, J. Mink, F. E. Kühn and C. C. Romão, *Organometallics*, 2003, **22**, 2112–2118.
22 A. A. Valente, J. D. Seixas, I. S. Gonçalves, M. Abrantes, M. Pillinger and C. C. Romão, *Catal. Lett.*, 2005, **101**, 127–130.
23 A. M. Al-Ajlouni, D. Veljanovski, A. Capapé, J. Zhao, E. Herdtweck, M. J. Calhorda and F. E. Kühn, *Organometallics*, 2009, **28**, 639–645.
24 D. Betz, A. Raith, M. Cokoja and F. E. Kühn, *ChemSusChem*, 2010, **3**, 559–562.
25 D. Betz, W. A. Herrmann and F. E. Kühn, *J. Organomet. Chem.*, 2009, **694**, 3320–3324.
26 K. R. Jain and F. E. Kühn, *Dalton Trans.*, 2008, 2221–2227.
27 *Aziridines and Epoxides in Organic Synthesis*, ed. A. K. Yudin, Wiley-VCH Weinheim, 2006.
28 K. R. Jain, W. A. Herrmann and F. E. Kühn, *Coord. Chem. Rev.*, 2008, **252**, 556–568.
29 J. A. Brito, B. Royo and M. Gómez, *Catal. Sci. Technol.*, 2011, **1**, 1109–1118.
30 F. E. Kühn, J. Zhao and W. A. Herrmann, *Tetrahedron: Asymmetry*, 2005, **16**, 3469–3479.
31 A. J. Burke, *Coord. Chem. Rev.*, 2008, **252**, 170–175.
32 M. Abrantes, A. Sakthivel, C. C. Romão and F. E. Kühn, *J. Organomet. Chem.*, 2006, **691**, 3137–3145.
33 M. Abrantes, F. A. A. Paz, A. A. Valente, C. C. L. Pereira, S. Gago, A. E. Rodrigues, J. Klinowski, M. Pillinger and I. S. Gonçalves, *J. Organomet. Chem.*, 2009, **694**, 1826–1833.
34 J. Zhao, E. Herdtweck and F. E. Kühn, *J. Organomet. Chem.*, 2006, **691**, 2199–2206.
35 J. K. P. Ariyaratne, A. M. Bierrum, M. L. H. Green, M. Ishaq, C. K. Prout and M. G. Swanwick, *J. Chem. Soc. A*, 1969, **1969**, 1309–1321.
36 L. R. Hillis and R. C. Ronald, *J. Org. Chem.*, 1981, **46**, 3348–3349.
37 G. R. Fulmer, A. J. M. Miller, N. H. Sherden, H. E. Gottlieb, A. Nudelman, B. M. Stoltz, J. E. Bercaw and K. I. Goldberg, *Organometallics*, 2010, **29**, 2176–2179.
38 *APEX suite of crystallographic software. APEX 2 Version 2008.4*, Bruker AXS Inc., Madison, Wisconsin, USA, 2008.
39 *SAINT, Version 7.56a and SADABS Version 2008/1*, Bruker AXS Inc., Madison, Wisconsin, USA, 2008.
40 G. M. Sheldrick, *SHELXS-97*, Program for Crystal Structure Solution, Göttingen, 1997.
41 G. M. Sheldrick, *SHELXL-97*, University of Göttingen, Göttingen, Germany, 1998.
42 C. B. Huebschle, G. M. Sheldrick and B. Dittrich, SHELXLE, *J. Appl. Crystallogr.*, 2011, **44**, 1281–1284.
43 *International Tables for Crystallography, Vol. C*, Tables 6.1.1.4 (pp. 500–502), 4.2.6.8 (pp. 219–222), and 4.2.4.2 (pp. 193–199), ed. A. J. C. Wilson, Kluwer Academic Publishers, Dordrecht, The Netherlands, 1992.
44 A. L. Spek, *PLATON*, A Multipurpose Crystallographic Tool, Utrecht University, Utrecht, The Netherlands, 2010.
45 E. R. Burkhardt, J. J. Doney, R. G. Bergman and C. H. Heathcock, *J. Am. Chem. Soc.*, 1987, **109**, 2022–2039.
46 R. B. King, M. B. Bisnette and A. Fronzaglia, *J. Organomet. Chem.*, 1966, **5**, 341–356.
47 T. S. Piper and G. Wilkinson, *J. Inorg. Nucl. Chem.*, 1956, **3**, 104–124.
48 R. B. King, *J. Organomet. Chem.*, 1975, **100**, 111–125.
49 R. B. King and A. Fronzaglia, *J. Am. Chem. Soc.*, 1966, **88**, 709–712.
50 J. K. P. Ariyaratne and M. L. H. Green, *J. Chem. Soc.*, 1964, 1–5.
51 L. J. Todd, J. R. Wilkinson, J. P. Hickey, D. L. Beach and K. W. Barnett, *J. Organomet. Chem.*, 1978, **154**, 151–157.
52 R. Mynott, H. Lehmkuhl, E.-M. Kreuzer and E. Joussen, *Angew. Chem., Int. Ed. Engl.*, 1990, **29**, 289–290.
53 R. F. Jordan, E. Tsang and J. R. Norton, *J. Organomet. Chem.*, 1978, **149**, 53–56.
54 J. W. Faller, A. S. Anderson and C.-C. Chen, *J. Chem. Soc. D*, 1969, 719–720.
55 R. Poli, *Organometallics*, 1990, **9**, 1892–1900.
56 J. M. Smith and N. J. Coville, *Organometallics*, 1996, **15**, 3388–3392.

57 C. G. Young, M. Minelli, J. H. Enemark, G. Miessler, N. Janietz, H. Kauermann and J. Wachter, *Polyhedron*, 1986, **5**, 407–413.
58 R. B. King and L. W. Houk, *Can. J. Chem.*, 1969, **47**, 2959–2964.
59 M. Abrantes, P. Neves, M. M. Antunes, S. Gago, F. A. Almeida Paz, A. E. Rodrigues, M. Pillinger, I. S. Gonçalves, C. M. Silva and A. A. Valente, *J. Mol. Catal. A: Chem.*, 2010, **320**, 19–26.
60 M. K. Trost and R. G. Bergman, *Organometallics*, 1991, **10**, 1172–1178.